JOURNAL OF GUIDANCE, CONTROL, AND DYNAMICS
Vol. 28, No. 2, March–April 2005

Optimization of Roundtrip, Time-Constrained, Finite Burn Trajectories via an Indirect Method

Chris L. Ranieri* and Cesar A. Ocampo†
University of Texas at Austin, Austin, Texas 78712

An indirect trajectory optimization method is used to compute optimal, time-constrained, roundtrip, finite burn trajectories between any two orbits around a common central body. This method involves solving the optimal control problem as a multipoint boundary value problem with two discontinuities in the controls corresponding to the arrival at and the departure from the target. Solutions are provided that minimize the propellant, given either an initial or final mass, while constraining the stay time at the target to be greater than or equal to a specified minimum value and while constraining the total roundtrip time to be less than or equal to a specified maximum value. The results are applied to human-crewed, one-year Earth–Mars roundtrip missions with a minimum two-month stay at Mars and four year Earth–Jupiter missions with a minimum one-year Jovian stay. These missions utilize high-power, nuclear electric propulsion with either a constant or variable specific impulse engine. This theoretical formulation was used to find quick, efficient, converged solutions that are shown to be at least as optimal or slightly more so compared to another optimization method that is hybrid in nature but still uses continuous control where the thrust is along the primer vector.

Nomenclature

c	=	exhaust velocity
$\boldsymbol{c}$	=	constraint vector for boundary value problem
G	=	Bolza function
$\boldsymbol{g}$	=	gravity acceleration vector
H	=	Hamiltonian
$\hat{\boldsymbol{h}}$	=	angular momentum unit vector for vehicle-centered frame
J	=	cost function
m	=	spacecraft mass
P	=	power
$\boldsymbol{R}$	=	rotation matrix from vehicle-centered to inertial frame
$\dot{\boldsymbol{R}}$	=	time derivative of rotation matrix from vehicle-centered to inertial frame
$\boldsymbol{r}$	=	spacecraft position vector
S	=	switching function
s_1	=	slack variable used with stay time constraint
s_2	=	slack variable used with total time of flight constraint
T	=	thrust
t	=	time
t_{stay}	=	stay time at target
$\boldsymbol{u}$	=	thrust unit vector
$\boldsymbol{u}_c$	=	control vector
$\dot{\boldsymbol{u}}$	=	thrust unit vector time derivative
$\boldsymbol{v}$	=	spacecraft velocity vector
$\hat{\boldsymbol{v}}$	=	velocity unit vector for vehicle-centered frame
$\hat{\boldsymbol{w}}$	=	third unit vector for vehicle-centered frame
$\boldsymbol{z}$	=	parameter vector for boundary value problem
α	=	in-plane thrust angle
β	=	out of plane thrust angle
$\boldsymbol{\theta}$	=	Lagrange multiplier adjoined with slack variables
$\boldsymbol{\lambda}$	=	costate Lagrange multiplier vector
λ_m	=	mass Lagrange multiplier
$\boldsymbol{\lambda}_r$	=	position costate Lagrange multiplier vector
λ_v	=	magnitude of velocity costate Lagrange multiplier vector
$\boldsymbol{\lambda}_v$	=	velocity costate Lagrange multiplier vector
$\dot{\lambda}_v$	=	time derivative of the magnitude of the velocity costate multiplier vector
μ_{CB}	=	central body's gravitational constant
$\boldsymbol{\Psi}$	=	kinematic constraints vector
$\boldsymbol{\omega}$	=	Lagrange multiplier adjoined with kinematic constraints

Subscripts

max	=	maximum value, power or thrust
Ti	=	spacecraft's target at time t_i, $i = 0, 1, 2, f$

Introduction

A SYSTEMATIC application of the indirect method is used to determine an optimal, minimum propellant, finite burn, roundtrip trajectory between any two orbits around a common central body. The roundtrip trajectory includes a specified minimum stay time at the target system, where the spacecraft coasts along with the target, simulating the time that could be used for human-crewed or robotic missions to visit the surface of the target or for a servicing satellite to perform its mission before returning back to its point of origin. This stay time is constrained to be greater than or equal to a minimum stay time at the target system. The total time of flight is constrained to be less than or equal to a specified maximum time of flight. The target system can be another spacecraft, a planet, a planetary system, moon, or any other celestial body that is orbiting the same central body as the spacecraft that is performing the transfer. A schematic of such a mission plan is given in Fig. 1.

The optimal control problem is solved as an indirect optimization problem; the associated Euler–Lagrange equations are integrated numerically, and the controls include the thrust direction and the constrained engine parameters. Two different optimization problems are solved, both aiming for minimum propellant missions. In the first, the initial spacecraft mass is specified and the final spacecraft mass on return to the point of origin is maximized. The second problem specifies the final spacecraft mass and minimizes the initial spacecraft mass at the departure from the point of origin. For both

Presented as Paper AAS03-572 at the AAS/AIAA Astrodynamics Specialist Conference, Big Sky, MT, 3–7 August 2003; received 1 October 2003; revision received 10 March 2004; accepted for publication 10 March 2004.

*National Defense Science and Engineering Graduate Research Fellow and Graduate Student, Department of Aerospace Engineering and Engineering Mechanics, 1 University Station C0600; cxr288@mail.utexas.edu.

†Assistant Professor, Department of Aerospace Engineering and Engineering Mechanics, 1 University Station C0600; cesar.ocampo@mail.utexas.edu.

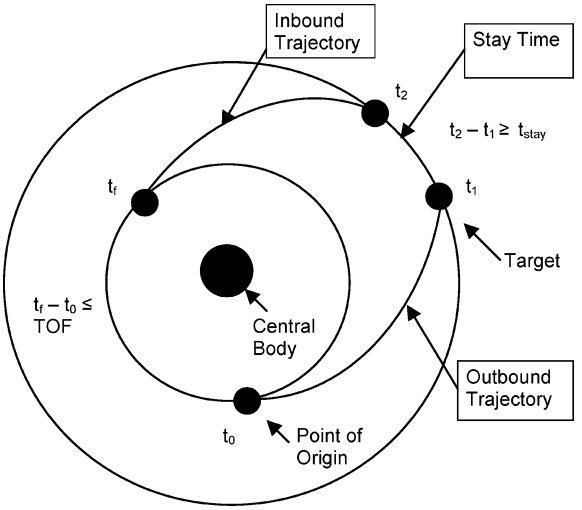

Fig. 1 Generalized roundtrip, time-constrained trajectory.

optimization problems, the start and end times of the inbound and outbound trajectories are free search variables. The resulting multipoint boundary value problem is solved by the use of the controls determined from the Pontryagin maximum principle.[1] The necessary first differential optimality conditions are determined when the aforementioned mission plan is considered as a trajectory with two control corner conditions, where the Lagrange multipliers that control the trajectory may or may not be continuous.

The first corner is at time t_1, which corresponds to the spacecraft's rendezvous with the target at the end of the outbound trajectory. The second corner is at time t_2, which corresponds to the departure time from the target at the end of the stay time trajectory. By combining the first differential optimality conditions generated at the initial and final times and at the two corners, with kinematic constraints such as the position and velocity of the target at time t_1 and t_2 and the position and velocity of the point of origin at t_0 and t_f, the trajectory can be optimized by solving a well-defined system of nonlinear equations. Additionally, an adjoint control transformation that uses control-related variables that have physical significance is used to help form a better estimate of the initial values for the unknown Lagrange multipliers.

The sample missions presented in this paper focus on high-power, fast roundtrip missions to Mars and Jupiter. In the coming decades, human-crewed missions to other planets in the solar system will become more feasible with the advent of more efficient and powerful spacecraft engines and propulsion systems. A promising propulsion device for such a class of trajectories is a high-power, variable specific impulse (VSI) engine. An example of this type of engine is the variable specific impulse magnetoplasma rocket (VASIMR) engine under development at the Advanced Space Propulsion Laboratory at the NASA Johnson Space Center.[2] In contrast to a constant specific impulse engine (CSI) engine, the variability of the specific impulse (I_{sp}) and thrust of a VSI engine increases the performance of these missions, providing higher payload mass fractions. The improved performance of VSI engines compared to CSI engines is demonstrated for the roundtrip Mars and Jupiter missions discussed in this study.

For the formulation of the roundtrip Mars mission, Earth and Mars are treated as zero sphere of influence point masses moving around the sun with a realistic ephemeris. The ephemeris used for this work is the three-dimensional, JPL DE405 ephemeris.[3] The trajectories are generated considering only the gravitational force from the sun on the spacecraft. For the VSI engine models, two finite burn arcs are used; the first burn arc is the outbound trajectory and the second burn arc is the inbound trajectory. For the finite burn CSI engine models, the inbound and outbound trajectories are modeled with three segments each: constant thrust arc/coast arc/constant thrust arc. This switching structure is explicitly assumed for these missions. Other switching structures with more thrusting and coast periods could produce better solutions that still satisfy all of the necessary conditions for optimality. However, the switching structure assumed here satisfies the first-order necessary conditions. The CSI engine models were set up to use the same power level as used in the VSI model with a chosen I_{sp} value representative of typical CSI engines. The power source is nuclear and bounded.

Roundtrip trajectories, particularly for interplanetary missions to Mars, have been solved previously by the use of a variety of methods. In contrast to previous studies, the current study uses the indirect method to formulate rigorously a multipoint boundary value problem that uses the corner conditions associated with the rendezvous with, and departure from, the target and includes both stay time and total trip time constraints.

Previously, roundtrip trajectories have been analyzed with direct methods. This technique involves parameterization of the controls and/or the states into a finite number of points instead of the use of the continuous solution generated by the indirect method. Solutions obtained with this method are generally considered suboptimal due to the discretization of either the states or controls, or both. The convergence of the direct method is generally more robust than that of the indirect method; however, for the problem considered here, the indirect method has a fairly rapid convergence, provided an adjoint control transformation is used. Direct methods are utilized by Ueno and Maruyama[4] in their work on optimizing roundtrip, time-constrained sample return missions to Mars. Kluever[5] and Kluever et al.[6] employ a direct method to parameterize the control rather than using the continuous control of the indirect method for both low thrust and impulsive missions. Direct methods are also used by Coverstone-Carroll and Williams,[7] Coverstone-Carroll et al.,[8] and Hargens and Coverstone-Carroll[9] in their work using differential inclusion to remove explicit control dependence from the problem formulation. Another version of the direct method, used by Tang and Conway,[10] is called direct collocation and nonlinear programming. This method removes the Lagrange multipliers and solves the boundary value problem by the use of piecewise continuous polynomials instead.

Analytical methods for determination of the optimal roundtrip mission have also been formulated that make some assumptions and simplifications to eliminate the numerical integration of the states and costates. Seywald et al.[11] use an analytic formulation to optimize orbital transfers using a VASIMR engine. Polsgrove and Adams[12] use a different analytical formulation to analyze roundtrip, high-power, interplanetary missions. However, these analytical methods are often limited in scope and must operate under a number of assumptions to be valid.

There also exist hybrid methods that numerically integrate the Euler–Lagrange equations and control the spacecraft based on the primer vector.[13,14] These hybrid formulations solve a nonlinear programming problem where the Lagrange multipliers of the indirect method and the relevant mission parameters form part of the parameter vector while extremizing a general scalar cost function.[13,14] Though some of the first differential optimal conditions associated with the indirect method can be included as equality constraints in the hybrid formulation, they are not necessary. Rather, it searches numerically for the set of parameters that drives the cost function to a numerical optimum point, while explicitly satisfying only the kinematic boundary constraints. One system that utilizes such a technique is COPERNICUS, a prototype generalized trajectory design and optimization tool currently under development at the University of Texas at Austin.[13,14] This hybrid tool was used to verify the numerical results found by the use of the indirect method.

As for indirect methods, they have been used in numerous papers to analyze one-way missions, but many examples are limited to search for fixed, specified initial and final time trajectories and do not consider the return leg as part of a complete, indirect optimal control formulation. These one-way missions have no discontinuities in either the states or controls. Vadali et al.[15] and Nah et al.[16] have performed research focused on optimizing fixed-time, one-way rendezvous trajectories with indirect methods. Their research does include the gravity of Earth and Mars in the problem formulation,

but does not include the stay time at Mars or the return leg in the indirect optimization problem.

Impulsive roundtrip interplanetary missions have been optimized with an indirect method by the use of the theory for state discontinuities as laid out by Bryson and Ho.[17] State discontinuities can be used for velocity impulses at the planets, as shown by Casalino et al.[18] and Pastrone et al.[19] A similar condition to the corner conditions necessary in the finite burning roundtrip mission posed here is the state and control discontinuity at a planetary gravity assist with a finite burning engine as analyzed by Casalino et al.[20] Casalino and Colasurdo,[21] and Casalino et al.[22]

Indirect methods that use calculus of variations optimization techniques have also been used by Sauer and Melbourne[23] and Melbourne et al.[24] in increasing degrees of complexity. Their work on roundtrip trajectories to Mars first involved the connection of two optimal, fixed transfer-time, one-way trajectories found with the indirect method to form the roundtrip trajectory. The optimal times for the initialization of each one way trajectory are found through geometric analysis of the motions of Earth and Mars. However, this does not address the full roundtrip trajectory as a single optimization problem. It does not search for the optimal starting times; rather, it explicitly analyzes the geometry of the orbits. It is also not free to search for the optimal split of outbound and inbound transfer times within the specified total time of flight bounds. However, this work has been further advanced and packaged in the program VARITOP at the Jet Propulsion Laboratory, California Institute of Technology (JPL), to optimize trajectories via the indirect method.[12,25] Research by Sauer[26] has addressed roundtrip missions using the indirect method without the restrictions on the flight times to search for the optimal outbound and inbound transfer times within the total time of flight bounds and the optimal starting times.

The formulation used in Sauer's work and VARITOP is similar to the method presented here. This paper, however, presents some insights and details into the time-constrained roundtrip trajectory not explicitly detailed in Sauer's research.[26] The main differences stem from the definition of the cost functions and, therefore, the Hamiltonian.[26] Additionally, this research rigorously derives and presents all of the necessary targeted conditions for optimality, detailing the behavior of the costates across the two corner control discontinuities at t_1 and t_2 and the effects of the inequality constraints on the stay time and total time of flight. The necessary conditions are formulated in terms of the switching function, which provides some tangible significance to the targeted conditions. Finally, the adjoint control transformation is introduced to improve the process of generating a good initial estimate of the unknown vector.

System Equations and the Optimal Control Problem

First, the equations of motion of the trajectory are defined:

$$\dot{\boldsymbol{X}} = \begin{bmatrix} \boldsymbol{v} \\ \boldsymbol{g} + (T/m)\boldsymbol{u} \\ \dot{m} = -T/c \end{bmatrix} \tag{1}$$

where

$$\boldsymbol{X} = \begin{bmatrix} \boldsymbol{r} \\ \boldsymbol{v} \\ m \end{bmatrix} \tag{2}$$

The force field is a time-invariant central body field:

$$\boldsymbol{g} = -\mu_{\mathrm{CB}}\boldsymbol{r}/r^3 \tag{3}$$

The thrust-direction unit vector is

$$|\boldsymbol{u}| = 1 \tag{4}$$

For a CSI engine, the controls are defined as the thrust direction and the thrust magnitude:

$$\boldsymbol{u}_c = \begin{bmatrix} \boldsymbol{u} \\ T \end{bmatrix} \tag{5}$$

$$0 \le T \le T_{\max} \tag{6}$$

For a VSI engine, the controls are the thrust direction, the thrust magnitude, and the power:

$$\boldsymbol{u}_c = \begin{bmatrix} \boldsymbol{u} \\ T \\ P \end{bmatrix} \tag{7}$$

$$0 \le P \le P_{\max} \tag{8}$$

There are two formulations for the cost function written in the Mayer form. The first maximizes the final mass at the return to the point of origin for a specified initial mass. This is equivalent to a minimum propellant problem:

$$\max J = m_f(\text{given } m_0) \tag{9}$$

The second cost function minimizes the initial mass for a specified final mass:

$$\max J = -m_0(\text{given } m_f) \tag{10}$$

The optimal control Hamiltonian and the costate equations are

$$H = \boldsymbol{\lambda}^T\dot{\boldsymbol{X}} = \boldsymbol{\lambda}_r^T\boldsymbol{v} + \boldsymbol{\lambda}_v^T\boldsymbol{g} + (T/m)\boldsymbol{\lambda}_v^T\boldsymbol{u} - (T/c)\lambda_m \tag{11}$$

$$-\dot{\boldsymbol{\lambda}}^T = \boldsymbol{H}_x \tag{12}$$

Equation (12) yields

$$\dot{\boldsymbol{\lambda}}_r = -\boldsymbol{\lambda}_v^T\left(\frac{\partial \boldsymbol{g}}{\partial \boldsymbol{r}}\right) \tag{13}$$

$$\dot{\boldsymbol{\lambda}}_v = -\boldsymbol{\lambda}_r \tag{14}$$

$$\dot{\lambda}_m = \frac{\lambda_v T}{m^2} \tag{15}$$

There are four sets of physical state constraints that must be met for a valid solution. The spacecraft must match the position and velocity of the target system at t_1 and t_2 and must also match the point of origin's position and velocity at t_0 and t_f:

$$\boldsymbol{\psi}_i = \begin{bmatrix} \boldsymbol{r}_{s/c}(t_i) - \boldsymbol{r}_{Ti}(t_i) \\ \boldsymbol{v}_{s/c}(t_i) - \boldsymbol{v}_{Ti}(t_i) \end{bmatrix} = \boldsymbol{0}, \qquad i = 0, 1, 2, f \tag{16}$$

The inequality constraints on the stay time at the target and on the total time of flight are treated via slack variables. They allow the program to search for the optimal stay time greater than a minimum prescribed stay time and a time of flight no longer than a prescribed total time of flight (TOF). Therefore, all of the times and the corresponding states in this problem formulation are free parameters:

$$t_2 = t_1 + t_{\text{stay}} + s_1^2 \tag{17}$$

$$t_f = t_0 + \text{TOF} - s_2^2 \tag{18}$$

These inequality constraints are then adjoined to the Bolza function with their own Lagrange multipliers. The Bolza function in the optimal control formulation includes the items that are being optimized and adjoins the kinematic boundary conditions via a set of new Lagrange multipliers. The Bolza function takes the form

$$G = m_f + \boldsymbol{\omega}_0^T\boldsymbol{\psi}_0 + \boldsymbol{\omega}_1^T\boldsymbol{\psi}_1 + \boldsymbol{\omega}_2^T\boldsymbol{\psi}_2 + \boldsymbol{\omega}_f^T\boldsymbol{\psi}_f + \theta_1\left(t_2 - t_1 - t_{\text{stay}} - s_1^2\right) + \theta_2\left(t_f - t_0 - \text{TOF} + s_2^2\right) \tag{19}$$

By the use of the partial derivative of the Hamiltonian with respect to the controls and the solution of the control variables, the Hamiltonian is maximized.[1] This results in the spacecraft thrust direction being aligned with the primer vector as defined by Lawden[27]:

$$\boldsymbol{u} = \boldsymbol{\lambda}_v/\lambda_v \tag{20}$$

For the CSI engine, the Hamiltonian is rewritten to group all of the thrust-dependent terms. Define the well known thrust switching function as

$$S = \lambda_v/m - \lambda_m/c \tag{21}$$

By substituting the primer vector and the switching function, the Hamiltonian is rewritten as

$$H = \boldsymbol{\lambda}_r^T \boldsymbol{v} + \boldsymbol{\lambda}_v^T \boldsymbol{g} + S \times T \tag{22}$$

For a CSI engine, to maximize the Hamiltonian, from the Pontryagin maximum principle, the well-known bang–bang switching structure is used to control the thrust times.[1] When the switching function is positive, the thrust is equal to its maximum value, and when the switching function is negative, thrust is set to zero. For VSI engines, the thrust magnitude is determined by maximization of the Hamiltonian. Although the Hamiltonian for a VSI engine is identical to that of a CSI engine, for the VSI engine it is rewritten to show its dependence on the three control variables: $\boldsymbol{u}$, thrust, and power. By the use of the primer vector and the exhaust velocity expressed in terms of power and thrust, it is

$$c = 2P/T \tag{23}$$

$$H = \boldsymbol{\lambda}_r^T \boldsymbol{v} + \boldsymbol{\lambda}_v^T \boldsymbol{g} + (T/m)\lambda_v - [T^2/(2P)]\lambda_m \tag{24}$$

The partial of the Hamiltonian with respect to the controls, thrust, and power is taken. Given that the thrust must always be greater than or equal to zero, the following conclusions are drawn:

$$T = P\lambda_v/(m\lambda_m) \tag{25}$$

$$P = P_{\max}, \qquad \lambda_m \geq 0 \tag{26}$$

$$P = 0, \qquad \lambda_m < 0 \tag{27}$$

The case with zero power is never actually possible for these missions because the mass multiplier will never have a negative value. As described in the Adjoint Control Transformation section, the initial mass multiplier is given an initial value of one. Additionally, the mass multiplier derivative is always nonnegative, as seen in Eq. (15). The thrust and the magnitude of the velocity multiplier are always nonnegative. Therefore, the mass multiplier will always be greater than zero for these missions, and the power will always be at the maximum value.

Optimality Conditions Across Control Corner Discontinuities

The conditions that must be satisfied for determination of the maximum mass at the end of the roundtrip trajectory are found by consideration of the preceding formulations for the CSI or VSI engines. The use of the first differential of the cost function yields the following conditions for optimality under the control of the primer vector and with the costates governed by the costate Eq. (12). The derivation of these conditions closely follows the corner conditions laid out by Hull[28] and Bryson and Ho.[17] The conditions with plus or minus subscripts correspond to the value of the variable before, for example, H_{1-}, or after, for example H_{1+}, the control corner at that time, such as t_1. The first cost function, Eq. (9) that maximizes the final mass, is used for this derivation. The differences in the derivation for the second cost function, Eq. (10), are explained after the first derivation is complete. The generalized cost function is

$$J = G + \int_{t0}^{tf} [H - \boldsymbol{\lambda}^T \dot{\boldsymbol{x}}]\, \mathrm{d}t \tag{28}$$

The conditions at the initial state and time t_0 are

$$G_{t0} = H_0 \tag{29}$$

$$G_{x0} = -\boldsymbol{\lambda}_0^T \tag{30}$$

The conditions at the first corner at t_1 are

$$G_{s1} = 0 = -2\theta_1 s_1 \tag{31}$$

$$G_{\theta 1} = 0 = t_2 - t_1 - t_{\text{stay}} - s_1^2 \tag{32}$$

$$G_{t1} = H_{1+} - H_{1-} \tag{33}$$

$$G_{x1} = \boldsymbol{\lambda}_{1-}^T - \boldsymbol{\lambda}_{1+}^T \tag{34}$$

The conditions at the second corner at t_2 are

$$G_{s2} = 0 = 2\theta_2 s_2 \tag{35}$$

$$G_{\theta 2} = 0 = t_f - t_0 - \text{TOF} + s_2^2 \tag{36}$$

$$G_{t2} = H_{2+} - H_{2-} \tag{37}$$

$$G_{x2} = \boldsymbol{\lambda}_{2-}^T - \boldsymbol{\lambda}_{2+}^T \tag{38}$$

The conditions at the final state and time t_f are

$$G_{tf} = -H_f \tag{39}$$

$$G_{xf} = \boldsymbol{\lambda}_f^T \tag{40}$$

Eqs. (31), (32), (35), and (36) correspond to the time constraints and their associated slack variables. With the two slack variables as unknowns, Eqs. (32) and (36) are directly utilized to solve for t_2 and t_f and, therefore, will always be satisfied. For both the CSI and VSI missions, the Hamiltonian is a constant across each leg of the trajectory because there are no terms in the Hamiltonian that are explicitly dependent on time. However, at the two corners, based on corner conditions in Eqs. (33) and (37), the Hamiltonian is not continuous. These results for the Hamiltonian were confirmed later for the actual missions optimized. By the use of the following simplifications, the necessary conditions for optimality are determined. Equation (40) is expanded as

$$G_{xf}^T = \begin{bmatrix} \boldsymbol{\omega}_{rf} \\ \boldsymbol{\omega}_{vf} \\ 1 \end{bmatrix} = \begin{bmatrix} \boldsymbol{\lambda}_{rf} \\ \boldsymbol{\lambda}_{vf} \\ \lambda_{mf} \end{bmatrix} \tag{41}$$

This shows that the mass multiplier is equal to unity at the final time:

$$\lambda_{mf} = 1 \tag{42}$$

With this information, the partial derivative of the Bolza function Eq. (19), with respect to the final time, yields

$$G_{tf} = -\boldsymbol{\omega}_{rf}^T \boldsymbol{v}_{Tf} - \boldsymbol{\omega}_{vf}^T \boldsymbol{g}_{Tf} + \theta_2 \tag{43}$$

$$G_{tf} = -\boldsymbol{\lambda}_{rf}^T \boldsymbol{v}_{Tf} - \boldsymbol{\lambda}_{vf}^T \boldsymbol{g}_{Tf} + \theta_2 \tag{44}$$

The Hamiltonian at the final time can be written as

$$H_f = \boldsymbol{\lambda}_{rf}^T \boldsymbol{v}_f + \boldsymbol{\lambda}_{vf}^T \boldsymbol{g}_f + S_f T_f \tag{45}$$

Ideally, when the spacecraft has achieved its target at the final time, the spacecraft and the target velocities will be identical, as will their gravitational accelerations. Therefore, the combination of Eqs. (44) and (45) as specified by Eq. (39) yields the following:

$$H_f + G_{tf} = S_f T_f + \theta_2 = 0 \tag{46}$$

Equation (30) is then expanded as

$$-G_{x0}^T = \begin{bmatrix} -\boldsymbol{\omega}_{r0} \\ -\boldsymbol{\omega}_{v0} \\ -\omega_{m0} \end{bmatrix} = \begin{bmatrix} \boldsymbol{\lambda}_{r0} \\ \boldsymbol{\lambda}_{v0} \\ \lambda_{m0} \end{bmatrix} \tag{47}$$

With this information, the partial derivative of the Bolza function Eq. (19), with respect to the initial time, yields

$$G_{t0} = -\boldsymbol{\omega}_{r0}^T \boldsymbol{v}_{T0} - \boldsymbol{\omega}_{v0}^T \boldsymbol{g}_{T0} - \theta_2 \tag{48}$$

$$G_{t0} = \boldsymbol{\lambda}_{r0}^T \boldsymbol{v}_{T0} + \boldsymbol{\lambda}_{v0}^T \boldsymbol{g}_{T0} - \theta_2 \tag{49}$$

The Hamiltonian at the initial time can be written as

$$H_0 = \boldsymbol{\lambda}_{r0}^T \boldsymbol{v}_0 + \boldsymbol{\lambda}_{v0}^T \boldsymbol{g}_0 + S_0 T_0 \tag{50}$$

The initial state of the spacecraft is specified to match the initial state of the point of origin, and, therefore, both will have identical velocities and gravitational accelerations at t_0. Combination of Eqs. (49) and (50) as specified by Eq. (29) yields the following:

$$H_0 - G_{t0} = S_0 T_0 + \theta_2 = 0 \tag{51}$$

Finally, Eqs. (46) and (51) can be combined to show that the switching function times the thrust must be equal at the initial and final times:

$$S_0 T_0 = S_f T_f \tag{52}$$

A similar simplification process is used across the two control corners. Equation (34) is expanded as

$$G_{x1}^T = \begin{bmatrix} \boldsymbol{\omega}_{r1} \\ \boldsymbol{\omega}_{v1} \\ 0 \end{bmatrix} = \begin{bmatrix} \boldsymbol{\lambda}_{r1-} - \boldsymbol{\lambda}_{r1+} \\ \boldsymbol{\lambda}_{v1-} - \boldsymbol{\lambda}_{v1+} \\ \lambda_{m1-} - \lambda_{m1+} \end{bmatrix} \tag{53}$$

This shows that the mass multiplier is continuous across the control corner discontinuity:

$$\lambda_{m1-} = \lambda_{m1+} \tag{54}$$

With this information in the partial derivative of the Bolza function, Eq. (19), with respect to the corner time t_1, yields

$$G_{t1} = -\boldsymbol{\omega}_{r1}^T \boldsymbol{v}_{T1} - \boldsymbol{\omega}_{v1}^T \boldsymbol{g}_{T1} - \theta_1 \tag{55}$$

$$G_{t1} = \left(\boldsymbol{\lambda}_{r1+}^T - \boldsymbol{\lambda}_{r1-}^T\right)\boldsymbol{v}_{T1} + \left(\boldsymbol{\lambda}_{v1+}^T - \boldsymbol{\lambda}_{v1-}^T\right)\boldsymbol{g}_{T1} - \theta_1 \tag{56}$$

The Hamiltonian before the corner subtracted from the Hamiltonian after the corner yields

$$H_{1+} - H_{1-} = \left(\boldsymbol{\lambda}_{r1+}^T - \boldsymbol{\lambda}_{r1-}^T\right)\boldsymbol{v}_1 + \left(\boldsymbol{\lambda}_{v1+}^T - \boldsymbol{\lambda}_{v1-}^T\right)\boldsymbol{g}_1 + S_{1+}T_{1+} - S_{1-}T_{1-} \tag{57}$$

Again, ideally when the spacecraft has achieved its target at the corner t_1, the spacecraft and the target velocities will be identical, as will their gravitational accelerations. Therefore, the combination of Eqs. (56) and (57) as specified by Eq. (33) yields the following:

$$S_{1+}T_{1+} - S_{1-}T_{1-} + \theta_1 = 0 \tag{58}$$

The derivation is almost exactly the same across the second corner. The mass multiplier is again continuous across the corner:

$$\lambda_{m2-} = \lambda_{m2+} \tag{59}$$

$$S_{2+}T_{2+} - S_{2-}T_{2-} - \theta_1 = 0 \tag{60}$$

Because the thrust at time t_{1+} and at time t_{2-} during the stay time at the target is always equal to zero, the terms with T_{1+} and T_{2-} can be dropped. Equations (58) and (59) reduce to

$$S_{1-}T_{1-} - \theta_1 = 0 \tag{61}$$

$$S_{2+}T_{2+} - \theta_1 = 0 \tag{62}$$

They can be further simplified to show that the switching function times the thrust must be equal at the end of the outbound leg and at the start of the inbound leg:

$$S_{1-}T_{1-} = S_{2+}T_{2+} \tag{63}$$

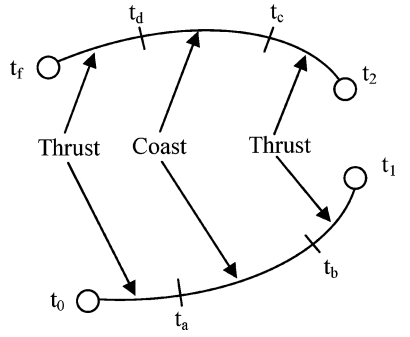

Fig. 2 Generalized CSI outbound and inbound legs: thrust/coast/thrust times.

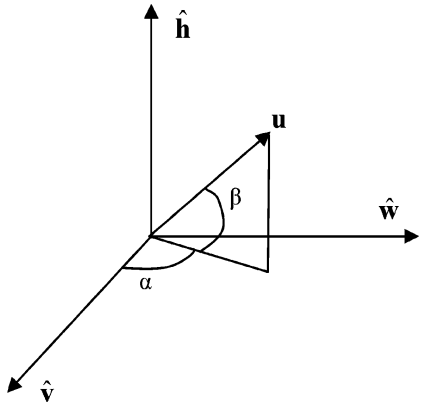

Fig. 3 Velocity-referenced frame for ACT.

For a CSI engine, there are four additional variables and constraints to consider. Because each leg of the CSI transfers is broken down into an assumed thrust/coast/thrust structure, the boundary value problem is set up to search explicitly for the switching times where the CSI engine switches from thrusting to coasting and vice versa. The variables t_a, t_b, t_c, and t_d represent the start and end of the coast periods for the outbound and inbound trajectories for a CSI engine. The corresponding constraints are that the switching function must be zero at these points. A generalized schematic of these times is shown in Fig. 2.

Adjoint Control Transformation

The initial estimates of the unknown vector can be refined and given more physical meaning with the use of an adjoint control transformation (ACT).[29] The velocity costates can be replaced by angles that describe the direction of the thrust. The initial magnitude of the velocity multiplier and its derivative are considered unknowns. These values can then be used to solve for the actual costate vector. This transformation is achieved first by expression of the thrust direction vector $\boldsymbol{u}$ in a vehicle-centered coordinate frame. For this example, a velocity-referenced coordinate frame is used. The three unit vectors that form the coordinate system are

$$\hat{\boldsymbol{v}} = \boldsymbol{v}/v \tag{64}$$

$$\hat{\boldsymbol{h}} = (\boldsymbol{r} \times \boldsymbol{v})/|\boldsymbol{r} \times \boldsymbol{v}| \tag{65}$$

$$\hat{\boldsymbol{w}} = \hat{\boldsymbol{h}} \times \hat{\boldsymbol{v}} \tag{66}$$

The thrust-direction unit vector $\boldsymbol{u}$ is written in this frame in terms of α and β in Fig. 3.

The thrust-direction unit vector in this frame is

$$\boldsymbol{u}_{vwh} = \begin{bmatrix} \cos\alpha\cos\beta \\ \sin\alpha\cos\beta \\ \sin\beta \end{bmatrix} \tag{67}$$

Its derivative, which is used in the transformation to the actual costates, is

$$\dot{\boldsymbol{u}}_{vwh} = \begin{bmatrix} -\dot{\alpha}\sin\alpha\cos\beta - \dot{\beta}\cos\alpha\sin\beta \\ \dot{\alpha}\cos\alpha\cos\beta - \dot{\beta}\sin\alpha\sin\beta \\ \dot{\beta}\cos\beta \end{bmatrix} \tag{68}$$

The thrust-direction unit vector is then rotated into the inertial coordinate frame utilized by the states and costates, which has its origin located at the problem's central body, for example, the sun.

$$\boldsymbol{u}_{ijk} = \boldsymbol{R}\boldsymbol{u}_{vwh} \tag{69}$$

$$\boldsymbol{R} = \begin{bmatrix} \hat{\boldsymbol{i}}\cdot\hat{\boldsymbol{v}} & \hat{\boldsymbol{i}}\cdot\hat{\boldsymbol{w}} & \hat{\boldsymbol{i}}\cdot\hat{\boldsymbol{h}} \\ \hat{\boldsymbol{j}}\cdot\hat{\boldsymbol{v}} & \hat{\boldsymbol{j}}\cdot\hat{\boldsymbol{w}} & \hat{\boldsymbol{j}}\cdot\hat{\boldsymbol{h}} \\ \hat{\boldsymbol{k}}\cdot\hat{\boldsymbol{v}} & \hat{\boldsymbol{k}}\cdot\hat{\boldsymbol{w}} & \hat{\boldsymbol{k}}\cdot\hat{\boldsymbol{h}} \end{bmatrix} \tag{70}$$

The first time derivative of this rotation matrix is required for use in the transformation to the actual costates. By the use of Eqs. (67), (68), and (70), along with the derivative of the rotation matrix, the derivative of the thrust-direction unit vector is expressed in the inertial frame:

$$\dot{\boldsymbol{u}}_{ijk} = \boldsymbol{R}\dot{\boldsymbol{u}}_{vwh} + \dot{\boldsymbol{R}}\boldsymbol{u}_{vwh} \tag{71}$$

Equation (20) can be rewritten to solve for the velocity multiplier vector as

$$\boldsymbol{\lambda}_v = \lambda_v \boldsymbol{u}_{ijk} \tag{72}$$

From the costate Eq. (12), because the gravity field is not a function of the velocity, the position multiplier vector can be written as

$$\boldsymbol{\lambda}_r = -\dot{\boldsymbol{\lambda}}_v \tag{73}$$

Taking the derivative of Eq. (72) and plugging it into Eq. (73), the position multiplier vector can be found:

$$\boldsymbol{\lambda}_r = -\dot{\lambda}_v \boldsymbol{u}_{ijk} - \lambda_v \dot{\boldsymbol{u}}_{ijk} \tag{74}$$

Additionally, the initial mass multiplier is set to one, which rescales the multipliers and eliminates an unknown from the search vector. The constraint, Eq. (42), that the final mass multiplier is equal to one is then dropped from the set of conditions. Because the mass multiplier derivative is always positive as described earlier, and the initial mass multiplier value is equal to one, the final mass multiplier will now equal some number greater than one. The cost function is multiplied by some positive constant K, greater than one, that in practical terms, is exactly the same cost function. The final mass multiplier value, which was originally one, is equal to K:

$$\max J = K m_f \tag{75}$$

$$\lambda_{m0} = 1 \tag{76}$$

$$\lambda_{mf} = K > 1 \tag{77}$$

Following this process, Eqs. (72), (74), and (76) directly provide the full costate vector. The new search variables become the initial angles for the thrust unit direction vector and their derivatives in a velocity-referenced, vehicle-centered frame. These unknowns have actual physical significance, and intelligent estimates can be made of these unknowns. The initial magnitude of the velocity multiplier and its derivative are also unknowns.

Boundary Value Problem

The preceding conditions and simplifications are now used to form a well-defined multipoint boundary value problem. The search vector for the problem with the adjoint control transformation is, for both engines,

$$\lambda_{m0} = 1 \tag{78}$$

for the CSI engine,

$$z_{\text{CSI}} = [t_0 \quad t_a \quad t_b \quad t_1 \quad \alpha_0 \quad \beta_0 \quad \dot{\alpha}_0 \quad \dot{\beta}_0 \quad \lambda_{v0} \quad \dot{\lambda}_{v0} \quad \ldots \quad s_1 \quad \theta_1 \quad s_2 \quad \theta_2 \quad \alpha_2 \quad \beta_2 \quad \ldots \quad \dot{\alpha}_2 \quad \dot{\beta}_2 \quad \lambda_{v2} \quad \dot{\lambda}_{v2} \quad t_c \quad t_d]^T_{22x1} \tag{79}$$

for the VSI engine,

$$z_{\text{VSI}} = [t_0 \quad t_1 \quad \alpha_0 \quad \beta_0 \quad \dot{\alpha}_0 \quad \dot{\beta}_0 \quad \lambda_{v0} \quad \dot{\lambda}_{v0} \quad s_1 \quad \ldots \quad \theta_1 \quad s_2 \quad \theta_2 \quad \alpha_2 \quad \beta_2 \quad \dot{\alpha}_2 \quad \dot{\beta}_2 \quad \lambda_{v2} \quad \dot{\lambda}_{v2}]^T_{18x1} \tag{80}$$

CSI necessary conditions are

$$\boldsymbol{c}_{\text{CSI}} = \begin{bmatrix} \boldsymbol{\psi}_{1\ 6x1} \\ \boldsymbol{\psi}_{f\ 6x1} \\ S_f T_f + \theta_2 \\ S_0 T_0 + \theta_2 \\ -2\theta_1 s_1 \\ 2\theta_2 s_2 \\ S_a \\ S_b \\ S_c \\ S_d \\ S_{t1-} T_{1-} - \theta_1 \\ S_{t2+} T_{2+} - \theta_1 \end{bmatrix}_{22x1} = \boldsymbol{0} \tag{81}$$

VSI necessary conditions are

$$\boldsymbol{c}_{\text{VSI}} = \begin{bmatrix} \boldsymbol{\psi}_{1\ 6x1} \\ \boldsymbol{\psi}_{f\ 6x1} \\ S_f T_f + \theta_2 \\ S_0 T_0 + \theta_2 \\ -2\theta_1 s_1 \\ 2\theta_2 s_2 \\ S_{t1-} T_{t1-} - \theta_1 \\ S_{t2+} T_{t2+} - \theta_1 \end{bmatrix}_{18x1} = \boldsymbol{0} \tag{82}$$

Minimizing Initial Mass for a Given Final Mass

In many cases for mission planning, it is desirable to specify a fixed final spacecraft mass and search for the minimum initial mass that can achieve the mission requirements and constraints. This allows a search to be performed for the minimum amount of propellant needed for a specific dry mass to complete a given mission. This is basically the same optimization problem as maximization of the final mass because the goal is to minimize the propellant, and the first-order optimal conditions are identical. However, the steps to generate those conditions are slightly different, and these differences are explained. By the use of the cost function as defined by Eq. (10), according to Eq. (30), the initial mass multiplier value is determined to have the value of one instead of an unknown constant as used in the maximum final mass case. However, this is exactly the same as the cases where the desire is to maximize the final mass for a given initial mass when the ACT is used where the multipliers are rescaled as described earlier. The final state condition, Eq. (40), then requires that the final mass multiplier is equal to some constant value, which necessarily is positive and greater than one. This is due to the mass multiplier derivative always being positive and the

initial mass multiplier value being equal to one. Again, this is identical to the maximum final mass problem when the ACT is used. The search vectors do slightly change for both CSI and VSI engines with the addition of the estimate of the initial mass. The additional constraint necessary to complete the boundary value problem is the difference between the specified final spacecraft mass and the final mass found of the trajectory.

Sample Missions

Solutions are generated by the use of a nonlinear boundary value solver from the Harwell Subroutine Library.[30] It is a hybrid algorithm that uses Newton–Raphson and steepest descent methods, combined with a Broyden method, to improve the Jacobian matrix to solve the multipoint boundary value problem. The set of sample missions presented here are for long-range, high-power, human-crewed missions to Mars and Jupiter. Both the VSI and CSI engines are powered by a 5-MW reactor. The CSI engine was set to operate at an I_{sp} of 5000 s. The VSI engine operates with no bounds on its I_{sp} or thrust levels. The total time of flight is constrained to be less than or equal to 365 days, whereas the stay time at Mars is constrained to be greater than or equal to 60 days. For the Jupiter missions, the maximum total TOF is four years, with a minimum one year stay time in the Jovian system. For all of the missions analyzed, the slack variables were driven to their constraint boundaries, that is, slack variables equal to zero, due to the short roundtrip mission times analyzed. The program reference epoch used in this program is a date chosen at random and does not necessarily correspond to a particularly favorable planetary alignment. The program then searches for the value of t_0 in days either before or after the reference epoch that yields the optimal starting time for the roundtrip trajectory. This tests the ability of the program to search for optimal solutions even when the initial estimate is far from the optimal solution.

Maximum Final Mass Trajectories

For both the Mars and Jupiter missions presented where the final mass is maximized, the initial mass is set at 100 mt. Figure 4 shows the optimal time constrained roundtrip Mars VSI trajectory.

Figure 5 shows the optimal time constrained roundtrip CSI trajectory to Mars. For the CSI engine, the thrust magnitude is constant. Figure 5 clearly shows the thrust/coast/thrust structure assumed for the CSI engine.

The maximum final mass values for both the CSI and VSI Mars and Jupiter missions are listed in Table 1. The VSI missions, as expected, are more fuel efficient than the CSI missions. However, the Mars CSI mission is much more efficient than the Jupiter CSI mission in comparison to the respective VSI missions to these planets. This is because the average VSI I_{sp} for the Jupiter missions is higher than the average VSI I_{sp} for the Mars trajectory. The CSI I_{sp} value of 5000 s was chosen to be representative of a capable CSI engine. It is not optimal, although for the Mars mission, it is closer to its optimal value than for the Jupiter mission. This is shown by the greater VSI fuel savings for the Jupiter mission in comparison to the Mars mission. The optimal I_{sp} for the CSI engine can only be found by the use of this program to perform a parametric scan of I_{sp} values for each particular mission.

Figures 6–8 show particular details for the Mars mission presented in Table 1. Figure 6 shows the plot of I_{sp} vs time for both the VSI and CSI engines. The CSI engine I_{sp} is constant at 5000 s. However, when the spacecraft is coasting, the I_{sp} is plotted in Fig. 6 as a value of zero to show the coast. The VSI I_{sp} is unbounded and takes values as high as 82,000 s to achieve the most optimal trajectory. The periods of extremely high VSI I_{sp} correspond to the coast periods of the CSI engine.

Figures 7 and 8 plot the switching function for the VSI and the CSI engines. Figures 7 and 8 clearly show that Eqs. (52) and (63) are

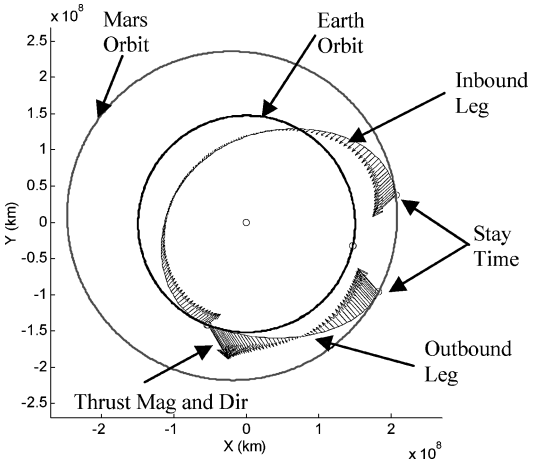

Fig. 4 VSI roundtrip human-crewed Mars mission ($t_0 = 30$ May 2018).

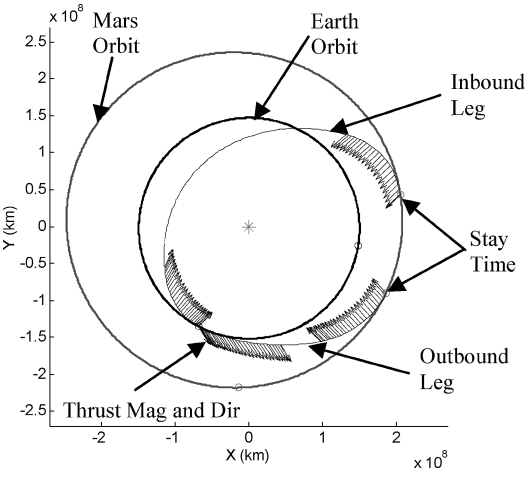

Fig. 5 CSI roundtrip human-crewed Mars mission ($t_0 = 24$ May 2018).

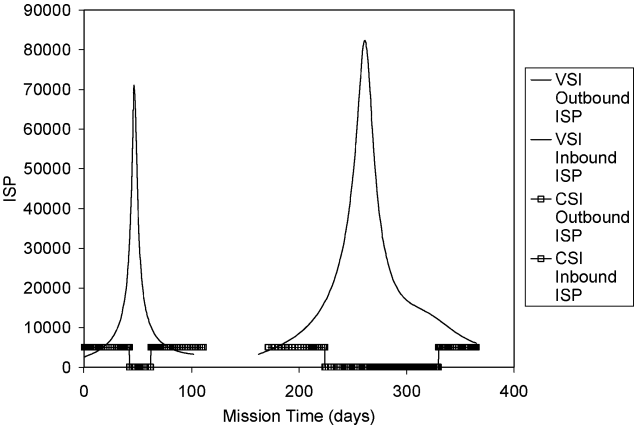

Fig. 6 VSI and CSI I_{sp} vs time.

Table 1 CSI and VSI maximum final mass ($m_0 = 100$ t)

Target body	Max TOF, days	Min stay time, days	CSI, $I_{sp} = 5000$ s, max m_f, kg	VSI max m_f, kg	VSI av I_{sp}, s	VSI fuel savings, kg
Mars	365	60	35,535	42,602	17,464	7,067
Jupiter	1460	365	38,766	60,782	42,604	22,016

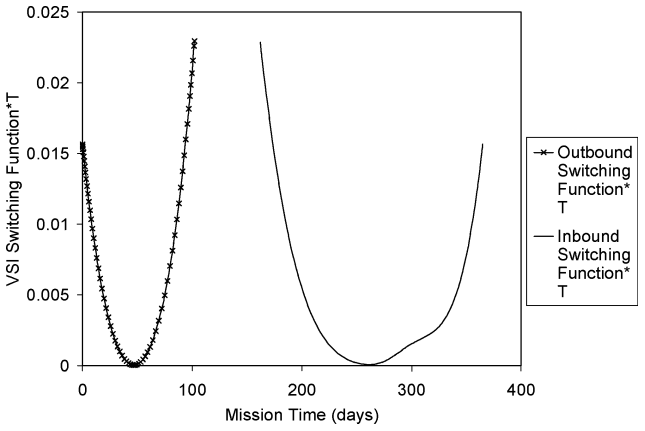

Fig. 7 VSI switching function times thrust vs mission time.

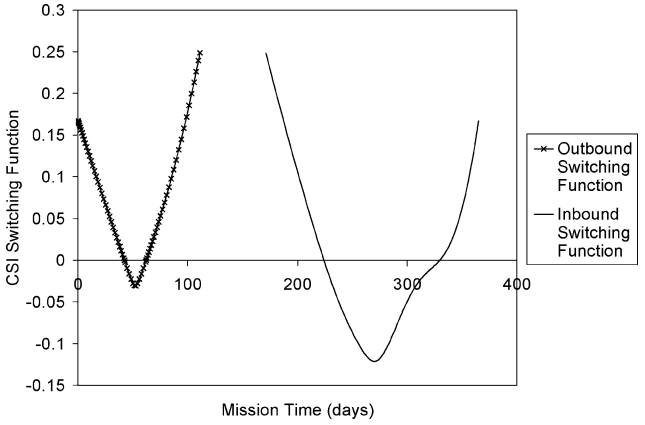

Fig. 8 CSI switching function vs mission time.

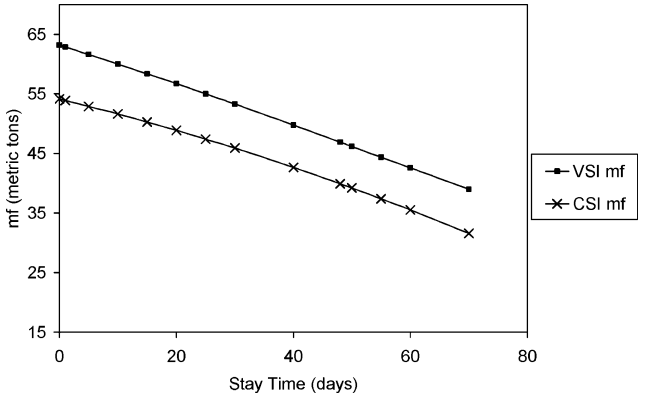

Fig. 9 Final mass vs martian stay time ($m_0 = 100$ t).

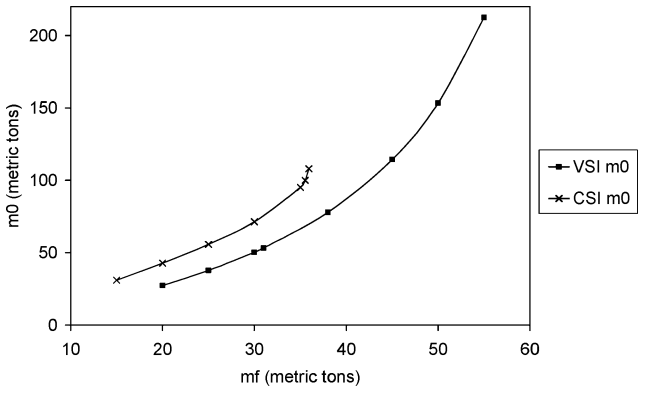

Fig. 10 Mars: CSI and VSI initial mass needed vs specified final mass.

satisfied. The initial and final values of the switching function times the thrust are equal. The values of the switching function times the thrust at the end of the outbound leg and the start of the inbound leg are also equal.

Figure 8 shows the CSI switching function and how that is used to control the trajectory and maximize the Hamiltonian. The times where the switching function crosses zero in Fig. 8 correspond to the final converged search variables t_a, t_b, t_c, and t_d. When the CSI switching function is negative, the spacecraft is on its coast arc.

VSI vs CSI Comparison

In a comparison of the VSI and CSI trajectories, the VSI trajectories are always more efficient in propellant usage. This behavior can be seen in Fig. 9 which shows the final mass on Earth return of a 100-t spacecraft with Martian stay times parametrically varied from 0 to 70 days. The VSI engine is 7000–9000 kg more efficient in fuel usage for each stay time.

Minimum Initial Mass Trajectories

When the cost function is switched to minimize the initial vehicle mass needed to achieve the mission with a specified final mass, prohibitive mission profiles are determined. A point is reached at which a specified final mass within the specified time bounds becomes completely unrealistic (VSI) or impossible (CSI). For the VSI engine, this point is for a much larger specified final mass value than is achievable for the CSI engine. The mission profile examined is again for a 365 day roundtrip mission with at least 60 days spent at Mars. The largest specified final mass VSI mission to converge was for a final mass of 74 t, and the corresponding minimum initial mass needed for this mission is almost 25,000 t, which is not a feasible initial mass. Figure 10 shows the initial mass needed to achieve the CSI and VSI missions plotted for a more realistic range of minimum initial mass values ($m_0 < 220$ t). Figure 10 very clearly shows the added controllability of the VSI engine vs the CSI engine. The CSI engine becomes uncontrollable as the slope tends toward infinity at a final mass of 36 t, much lower than the achievable specified final mass of 74 t (not shown) for the VSI engine. If final mass values greater than 36 t is required for the CSI engine, the I_{sp} would have to be lowered to allow the engine greater thrust capabilities to accommodate the larger vehicle mass.

Verification of Results

To verify the numerical results produced with the indirect method, the Mars missions presented in this paper were optimized independently with COPERNICUS. As described earlier, COPERNICUS currently uses a hybrid algorithm to determine optimal roundtrip trajectories.[13,14] The amount of propellant used in these missions ranged from 40,000 to 65,000 kg of fuel. For the maximum final mass, a one-year roundtrip Mars mission with a 60-day stay time, for the VSI engine, COPERNICUS and this program had a difference of 0.07 kg of propellant. This is only a $1.2E-4\%$ difference in propellant mass. For the same CSI mission, the result found from the indirect method was 263 kg more efficient in propellant usage compared to COPERNICUS. This is still a very small difference in fuel usage, or a 0.38% difference. The agreement of these results proves that the indirect method applied to the time-constrained, roundtrip mission is capable of generating accurate, reliable optimal solutions.

Conclusions

The indirect method, which accounts for control discontinuities at the arrival and departure from the target, has been shown to generate roundtrip solutions efficiently that satisfy all of the necessary conditions for optimality. Use of the ACT allows intelligent initial estimates to be formed, leading to quick convergence. The numerical results generated by the use of these optimality conditions are verified with an independent hybrid optimization tool that produces practically identical minimum propellant mass values. The missions presented could be useful in mission planning for the proposed human-crewed missions to the moon and Mars in the coming

decades. Additionally, this methodology, although applied to missions that are currently not feasible, can be applied to a wide range of other near-term missions such as robotic sample return missions to planets, comets, or asteroids with much smaller vehicles and propulsion systems.

More details can be added to the current model to make it more realistic and robust. Realistic upper and lower bounds will be placed on the specific impulse and thrust of the variable specific impulse engine to represent more accurately the true capabilities of such an engine. It is also envisioned that the optimal control problem be reformulated to account for a mass discontinuity at the target to simulate spacecraft mass left at the target system. A minimum heliocentric distance constraint may be imposed to limit the spacecraft from approaching the sun too closely. A final goal is the analysis of missions where the time slack variables are not driven to their boundaries by the dynamics of the system and the stringent total transfer-time constraint.

References

[1]Pontryagin, L. S., Boltyanskii, V. G., Gamkrelidze, R. V., and Mishchenko, E. F., *The Mathematical Theory of Optimal Processes*, Wiley-Interscience, New York, 1962, pp. 9–65.

[2]Chang-Diaz, F., "The VASIMR Rocket," *Scientific American*, Vol. 283, No. 5, 2000, pp. 90–97.

[3]Standish, E. M., "JPL Planetary Ephemirides," Jet Propulsion Lab., California Inst. of Technology [online], URL: http://ssd.jpl.nasa.gov/eph_info.html/ [cited 18 Sept. 2003].

[4]Ueno, S., and Maruyama, R., "Minimum Fuel Trajectories for Sample-Return Mission Using Solar Electoric Propulsion," *Journal of Space Technology and Science*, Vol. 16, No. 2, 2000, pp. 24–34.

[5]Kluever, C. A., "Simple Control Laws for Low-Thrust Orbit Transfers," *Advances in the Astonautical Sciences*, Vol. 99, Pt. 2, Univelt, Inc., San Diego, CA, 1998, pp. 1455–1468.

[6]Kluever, C. A., Cupples, M. L., and Kirchmyer, R. H., "A Direct Trajectory Optimization Method For Constrained Interplanetary Missions," *Advances in the Astronautical Sciences*, Vol. 102, Pt. 1, 1999, pp. 423–430.

[7]Coverstone-Carroll, V., and Williams, S. N., "Optimal Low Thrust Trajectories Using Differential Inclusion Concepts." *Journal of Astronautical Sciences*. Vol. 42, No. 4, 1994, pp. 379–393.

[8]Coverstone-Carroll, V., Hartman, C. A., Herman, A. L., and Spencer, D. B., "Optimal Spacecraft Trajectories Via Higher Order Differential Inclusion," *Advances in the Astronautical Sciences*, Vol. 102, Pt. 1, 1999, pp. 377–395.

[9]Hargens, J. J., and Coverstone-Carroll, V., "Low-Thrust Interplanetary Mission Design Using Differential Inclusion," *Proceedings of the AIAA/AAS Astrodynamics Conference*, AIAA, Reston, VA, 2002.

[10]Tang, S., and Conway, B. A., "Optimization of Low-Thrust Interplanetary Trajectories Using Collocation and Nonlinear Programming," *Journal of Guidance, Control, and Dynamics*, Vol. 18, No. 3, 1995, pp. 599–604.

[11]Seywald, H., Troitmayr, C. M., and Troutman, P. A., "Fuel-Optimal Orbital Transfers For Variable Specific Impulse Power Spacecraft," *Advances in the Astronautical Sciences*, Vol. 114, 2003, pp. 347–364.

[12]Polsgrove, T., and Adams, R. B., "Trajectories For High Specific Power Deep Space Exploration," *Proceedings of the AIAA/ASME/SAE/ASEE Joint Propulsion Conference and Exhibit*, AIAA, Reston, VA, 2002.

[13]Ocampo, C., "An Architecture for a Generalized Trajectory Design and Optimization System," *Proceedings of the International Conference on Libration Points Orbits and Applications*, Parador d'Aiguablava, Girona, Spain, 2002, pp. 529–571.

[14]Ocampo, C., "Finite Burn Maneuver Modeling for a Generalized Spacecraft Trajectory Design and Optimization System," *Astrodynamics, Space Missions, and Chaos, Annals of the New York Academy of Sciences*, Vol. 1017, May 2004.

[15]Vadali, S. R., Nah, R., Braden, E., and Johnson, I. L., Jr., "Fuel-Optimal Planar Interplanetary Trajectories Using Low-Thrust Exhuast-Modulated Propulsion," *Advances in the Astronautical Sciences*, Vol. 102, Pt. 1, 1999, pp. 431–441.

[16]Nah, R. S., Vadali, S. R., and Braden, E., "Fuel Optimal, Low-Thrust, Three-Dimensional Earth–Mars Trajectories," *Journal of Guidance, Control, and Dynamics*, Vol. 24, No. 6, 2001, pp. 1100–1107.

[17]Bryson, A., and Ho, Y. C., *Applied Optimal Control: Optimization, Estimation, and Control*, Hemisphere, New York, 1975, pp. 90–128.

[18]Casalino, L., Colasurdo, G., and Pastrone, D., "Optimization Procedure for Preliminary Design of Opposition-Class Mars Missions," *Journal of Guidance, Control, and Dynamics*, Vol. 21, No. 1, 1998, pp. 134–140.

[19]Pastrone, D., Casalino, L., and Colasurdo, G., "Indirect Optimization For Round-Trip Mars Trajectories," *Advances in the Astronautical Sciences*, Vol. 90, Pt. 1, 1995, pp. 85–99.

[20]Casalino, L., Colasurdo, G., and Pastrone, D., "Optimal Low-Thrust Escape Trajectories Using Gravity Assist," *Journal of Guidance, Control, and Dynamics*, Vol. 22, No. 5, 1999, pp. 637–641.

[21]Casalino, L., and Colasurdo, G., "Optimization of Variable-Specific-Impulse Interplanetary Trajectories," *Proceedings of the AIAA/AAS Astrodynamics Conference*, AIAA, Reston, VA, 2002.

[22]Casalino, L., Colasurdo, G., and Pastrone, D., "Optimal Low-Thrust Trajectories Using Flyby," *Advances in the Astronautical Sciences*, Vol. 99, Pt. 2, 1998, pp. 1409–1423.

[23]Sauer, C. G., Jr., and Melbourne, W. G., "Optimum Earth-to-Mars Roundtrip Trajectories Utilizing a Low-Thrust Power-Limited Propulsion System," *Advances in the Astronautical Sciences*, Vol. 13, 1963, pp. 547–570.

[24]Melbourne, W. G., and Richardson, D. E., and Sauer, C. G., "Interplanetary Trajectory Optimization with Power-Limited Propulsion Systems," Jet Propulsion Lab., California Inst. of Technology, TR 32-173, Pasadena, CA, Feb. 1962.

[25]Williams, S. N., and Coverstone-Carroll, V., "Mars Missions Using Solar Electric Propulsion," *Journal of Spacecraft and Rockets*, Vol. 37, No. 1, 2000, pp. 71–77.

[26]Sauer, C. G., Jr., "Optimization of Multiple Target Electric Propulsion Trajectories," *Proceedings of the AIAA 11th Aerospace Sciences Meeting*, AIAA, New York, 1973.

[27]Lawden, D. F., *Optimal Trajectories for Space Navigation*, Butterworths, London, 1963, pp. 79–94.

[28]Hull, D. G., *Optimal Control Theory for Applications*, Springer, New York, 2003, pp. 276–316.

[29]Dixon, L. C., and Bartholomew-Biggs, M. C., "Adjoint Control Transformations for Solving Practical Optimal Control Problems," *Optimal Control Applications and Methods*, Vol. 2, Oct.–Dec. 1981, pp. 365–381.

[30]"NS11AD-ns11.pdf," Harwell Subroutine Library [online numerical library], URL: http://www.cse.clrc.ac.uk/nag/hsl/ [cited 18 July 2003].